


SCIENTIFIC REPORTS



OPEN

Numerical Simulation of Particulate Matter 2.5 Distribution in a Roadway

Guorui Feng^{1,2}, Qi Liao¹ & Shengyong Hu ^{1,2}

Large amounts of dust particles pose serious hazards to the health and safety of China's coal miners during roadway blasting processes. It is known that among these dust particles, Particulate Matter 2.5 (PM_{2.5}) does the greatest amount of harm. In order to study the distributions of the PM_{2.5} in roadway blasting processes, a mathematical model of the gas-solid two-phase flow was established in this study, which was based on a Direct Simulation Monte Carlo Method (DSMC). Then, a multiphase flow program was developed. This study's results indicated that following the blasting processes, fine dust particles gradually floated up and were suspended for long durations in the underground roadway space. The medium-sized dust particles slowly sink to the ground and were eventually expelled before settling to the floor of the roadway. The coarse particles were rapidly settled to the roadway floor. It was determined that the PM_{2.5} particles in the front end of the dust group could not be quickly diluted, and the concentrations were high until it is expelled from the roadway, whereas the PM_{2.5} dust particles in the back end of the underground roadway were found to be gradually diluted. Eventually, the PM_{2.5} concentrations exhibited an alternating thin to dense phase distribution. When compared with the Particulate Matter 5 (PM₅), it was found that the PM_{2.5} was more difficult to discharge, and easily formed serious PM_{2.5} dust air pollution. This study's results were determined to be conducive to the future control of PM_{2.5} in the underground roadway blasting processes.

Recently, cases of pneumoconiosis in China have been increasing by 25,000 each year, and there have been more than 6,000 deaths as the result of coal dust inhalation¹. Mining operations, such as underground roadway blasting processes, tend to generate dust in both the respirable and non-respirable size range². Respirable dust is a main factor which has led to coal workers' pneumoconiosis³. PM_{2.5} is classified as a respirable dust, and is known to have toxic effects on the cardiovascular system by directly entering into the human pulmonary alveolus⁴. Therefore, in order to ensure the health and safety of China's miners, more attention should be paid to the PM_{2.5} dust particles generated in underground roadway blasting processes.

At the present time, PM_{2.5} is being widely studied in atmospheric environments all over the world⁵⁻⁷. There is no standard of PM_{2.5} concentration in the dust control of coal mines. In order to control PM_{2.5} pollution in coal mines, a ground atmospheric standard for PM_{2.5} was introduced⁸⁻¹⁰. Meanwhile, the PM_{2.5} in coal mines is different in concentration and composition, as well as other aspects¹¹. Therefore, examining the distributions of PM_{2.5} in coal mines has become a very urgent matter.

Numerical simulation is a highly efficient method which has been widely adopted to study dust distributions in coal mines¹². Nie *et al.*¹³ used Fluent software to simulate the total dust migration regulations of full rock excavation roadway under different airflow rates. Also, Niu *et al.*¹⁴ conducted a study regarding the movement behaviors of respirable dust, as well total dust distributions in mine excavation face using Fluent software. Toraño *et al.*¹⁵ utilized CFD software to evaluate total dust distribution regulations with two types of local ventilation methods in a fully mechanized mining face. Kurnia *et al.*¹⁶ conducted a study regarding the distribution of dust particles with different diameters in excavation face with different ventilation modes using CFD software. Wang *et al.*¹⁷ used a discrete phase model to simulate the total concentrations of dust and respirable dust in the ventilation processes of the roadway working faces in coal mine. Qin *et al.*¹⁸ studied the dust distributions in excavation roadways with dust removal and ventilation systems which is long pinging and short pressing, using Fluent software. Nie *et al.*¹⁹ applied Fluent software to study the changes in airflow fields in hard rock mechanized mining faces. Chen *et al.*²⁰

¹College of Mining Engineering, Taiyuan University of Technology, Taiyuan, 030024, China. ²Green Mining Engineering Technology Research Center of Shanxi Province, Taiyuan, 030024, China. Correspondence and requests for materials should be addressed to S.H. (email: hsyzt@163.com)

applied Fluent software to simulate the dust distributions following stope blasting processes. However, the aforementioned research studies were mainly focused on the distributions of the total dust or respirable dust in the mechanized working faces of mines. To date, very little attention has been paid to the distributions of PM_{2.5} particles in underground roadways following mine blasting processes.

Therefore, in order to address this issue, a gas particle two-phase flow model was developed in this study for the examination of PM_{2.5} distributions and the resulting air pollution hazards in underground mining roadways following blasting processes.

Method

Gas-solid two-phase models. The discrete particle phase was studied in this study based on the Euler method. The continuous gas phase was studied based on the Lagrange method. This study also studied the gas-solid two-phase flow following blasting processes. Furthermore, based on the DSMC method, the collisions between particles were taken into consideration. Due to the relatively low concentrations of the particle phase, the coupling effects between the gas and solid phases were neglected in this study's investigations, and only the effects of the gas phase on the solid phase were considered²¹. The momentum equation of the gas phase, along with the equation of continuity were presented as follows²²:

$$\begin{cases} \frac{\partial(u_j)}{\partial(x_j)} = 0 \\ \frac{\partial(u_i)}{\partial t} + \frac{\partial(u_i u_j)}{\partial x_j} = \frac{1}{\rho_g} \left(-\frac{\partial p}{\partial x_i} + \frac{\partial(\tau_{ji})}{\partial x_j} + \rho_g g \right) \end{cases} \quad (1)$$

where τ_{ji} represents the turbulent stress tensor; u_j and u_i denote the velocity; and $i, j = 1, 2, 3$ represent the x, y , and z directions, respectively; t represents the unit vector in the tangential direction; ρ_g is gas phase density; g is gravitational acceleration.

$$\tau_{ji} = (\mu + \mu_t) \left(\frac{\partial u_j}{\partial x_i} + \frac{\partial u_i}{\partial x_j} \right) - \frac{2}{3} \rho_g \kappa \delta_{ij} \quad (2)$$

where δ_{ij} represents the Kronecker constant; κ represents the turbulent kinetic energy; μ_t denotes the turbulent viscosity; and μ denotes the dynamic viscosity.

The forces on the particle phase were mainly considered, including the forces of the particle-particle interactions; forces of the particle-wall interactions; and forces of the particles and airflow^{23,24}. There were multiple forces of particle-gas interactions present, including the Basset, Magnus, Saffman, pressure gradient, false quality, and drag forces. However, the gravity force was only considered among the field forces. Also, only the drag force was taken into consideration among the fluid forces. The related equations were as follows:

$$f_d = \beta(v - u) \quad (3)$$

$$u_r = u - v \quad (4)$$

where f_d represents the drag force; v is the solid phase velocity; and u is the gas velocity.

$$Re = D_p |u_r| / \nu \quad (5)$$

$$\beta = \frac{3}{4} C_D \frac{|v - u| \rho (1 - \varepsilon)}{D_p} \varepsilon^{-2.7} \quad (6)$$

where Re is Reynolds number; D_p represents the particle diameter; ε is the voltage; and ρ is the gas phase density.

$$C_D = \begin{cases} 24(1 + 0.15Re^{0.687})/Re & Re \leq 1000 \\ 0.43 & Re > 1000 \end{cases} \quad (7)$$

Then, the trajectories of the sample particles were studied based on the DSMC model. Due to the effects of the particle rotations, the particle-particle collisions were determined using probability. The related equations were as follows:

$$m_1(V_1 - V_1^{(0)}) = J \quad (8)$$

$$m_2(V_2 - V_2^{(0)}) = -J \quad (9)$$

where m is the mass; J is the impulse exerted on Particle 1, acts on Particle 2 as the reaction; V represents the velocity. In the following two equations, the subscripts 1 and 2 represent the two particles. Also, the superscript (0) represents the values before collision.

$$I_1(\omega_1 - \omega_1^{(0)}) = r_1 n \times J \quad (10)$$

$$I_2(\omega_2 - \omega_2^{(0)}) = r_2 n \times J \quad (11)$$

where I represents rotational inertia of particle; r stands for the particle radius; and n stands for the normal unit vector directed from Particle 1 to Particle 2 at the moment of contact.

$$\frac{n \cdot G^{(0)}}{|G_{ct}^{(0)}|} > \frac{2}{7} \frac{1}{f(1+e)} \quad (12)$$

$$V_1 = V_1^{(0)} - \left[(1+e)(n \cdot G^{(0)})n + \frac{2}{7}|G_{ct}^{(0)}|t \right] \frac{m_2}{m_1 + m_2} \quad (13)$$

$$V_2 = V_2^{(0)} + \left[(1+e)(n \cdot G^{(0)})n + \frac{2}{7}|G_{ct}^{(0)}|t \right] \frac{m_1}{m_1 + m_2} \quad (14)$$

$$\omega_1 = \omega_1^{(0)} - \frac{5}{7r_1}|G_{ct}^{(0)}|(n \times t) \frac{m_2}{m_1 + m_2} \quad (15)$$

$$\omega_2 = \omega_2^{(0)} - \frac{5}{7r_2}|G_{ct}^{(0)}|(n \times t) \frac{m_1}{m_1 + m_2} \quad (16)$$

$$\frac{n \cdot G^{(0)}}{|G_{ct}^{(0)}|} < \frac{2}{7} \frac{1}{f(1+e)} \quad (17)$$

$$V_1 = V_1^{(0)} - (n - ft)(n \cdot G^{(0)})(1+e) \frac{m_2}{m_1 + m_2} \quad (18)$$

$$V_2 = V_2^{(0)} + (n - ft)(n \cdot G^{(0)})(1+e) \frac{m_1}{m_1 + m_2} \quad (19)$$

$$\omega_1 = \omega_1^{(0)} + \frac{5}{2r_1}(n \cdot G^{(0)})(n \times t)f(1+e) \frac{m_2}{m_1 + m_2} \quad (20)$$

$$\omega_2 = \omega_2^{(0)} + \frac{5}{2r_2}(n \cdot G^{(0)})(n \times t)f(1+e) \frac{m_1}{m_1 + m_2} \quad (21)$$

where f refers to the friction coefficient of the Coulomb Friction Law; and e refers to the coefficient of the restitution.

$$G^{(0)} = V_1^{(0)} - V_2^{(0)} \quad (22)$$

$$G_{ct}^{(0)} = G^{(0)} - (G^{(0)} \cdot n)n + r_1\omega_1^{(0)} \times n + r_2\omega_2^{(0)} \times n \quad (23)$$

$$t = \frac{G_{ct}^{(0)}}{|G_{ct}^{(0)}|} \quad (24)$$

where $G^{(0)}$ is the relative velocity of the particle centers before collision occurs; $G_{ct}^{(0)}$ denotes the tangential component of the $G^{(0)}$ of the contact point prior to collision occurring.

In this study, the roadway wall was regarded as an infinite sphere. A particle-to-particle collision model was established to deal with the collisions between the particles and roadway wall. Then, the corresponding program development of the particle movements was independently completed.

Geometrical model. The Wulan Coal Mine is located in the Ningxia Hui Autonomous Region of China. Large amounts of coal dust are produced during the working face blasting processes in the Wulan Coal Mine due to its soft coal seam. These coal dust particles float in the air with an average concentration of 1,500 mg/m³. A working face in China's Wulan Coal Mine was selected as a physical prototype, as shown in Fig. 1. The study area's underground rectangular roadway was 4 m in width, and had a height of 3 m. The ventilation duct which was located in the underground roadway had a 0.8 m diameter. The distance from the outlet of the ventilation duct to the working face was 14 m, and was 0.3 m from the roof. The airflow velocity in the outlet of ventilation duct was 10 m/s. The coal dust spray following the blasting had a speed of 6 m/s. Table 1 lists the simulation parameters of this study's geometric model.

Simulation parameters	Value
Air viscosity (m ² /s)	0.000017894
Air density (kg/m ³)	1.225
Dust density (kg/m ³)	1500
Time step for particle (s)	0.000025
Simulated particles flow time (s)	180
Initial dust concentration (mg/m ³)	1500
Particle median diameter	0.000055
Particle dispersion index	2.95
Maximum particle diameter (μm)	100
Minimum particle diameter (μm)	0.1
Gas phase grid number	530000
Coefficient of restitution between particles	0.8
Coefficient of restitution between particle and wall	0.6
Friction coefficient between particles	0.3
Friction coefficient between particle and roadway wall	0.4

Table 1. Calculation model parameters.

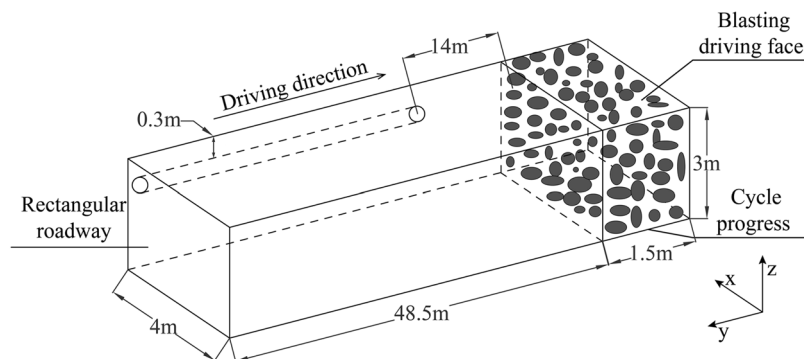


Figure 1. Geometric model of the blast driven roadway.

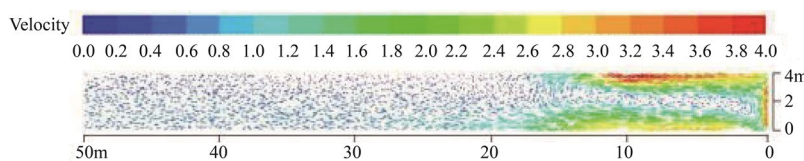


Figure 2. Velocity distributions of airflow fields in the breathing zone.

Results and Discussion

Airflow fields. In order to study the airflow fields in the study area after the blasting processes, the ordinate $Z = 1.5$ was taken as the height of the breathing zone. Figure 2 shows the velocity distributions in the breathing zone following the blasting processes.

As shown in Fig. 2, within the front-end of the roadway, the airflow velocity was approximately 3.2 m/s. Its maximum value on the left-hand side of the roadway was 4 m/s, while it was 2.8 m/s on the right. Near the left wall of the front-end, the direction of the blasting shock wave was the opposite of the airflow. Therefore, the airflow velocity near the left wall of the front-end was significantly lower than that in the outlet of the ventilation duct. Due to the viscous effects, the airflow velocities around the blast working face and close to the right wall were obviously lower than those on the left-hand side.

In the roadway areas ranging from 0 to 25 m away from the driving face, an obvious vortex region with a banded vortex center was obvious. The airflow velocity in the vortex center was approximately 0.4 m/s, which was significantly lower than that close to the blast driven face and near both sides of the underground roadway. In the regions located more than 25 m from the driven face of the coal mine roadway, the airflow velocity gradually became weakened to below 1.0 m/s. This was found to be due to the friction between the roadway wall

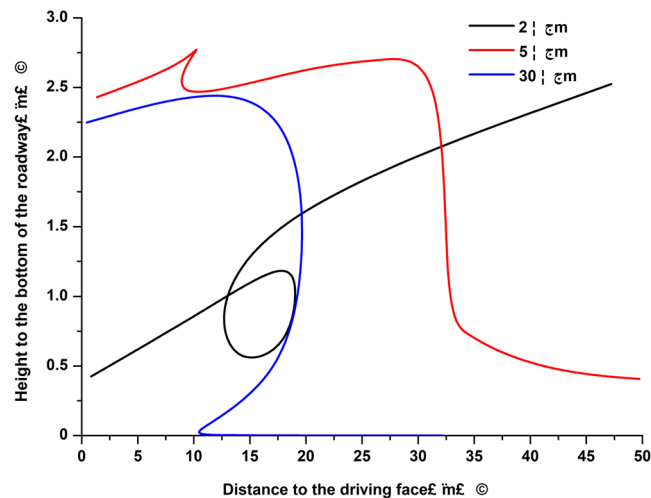


Figure 3. Contrasts in the trajectories of the different particle sizes.

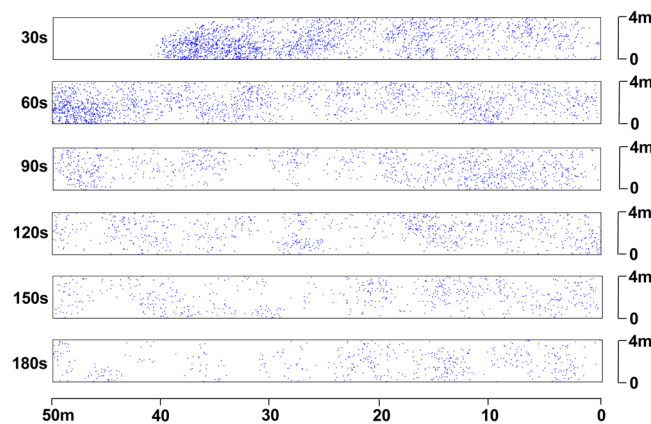


Figure 4. $PM_{2.5}$ particle distributions within the breathing zone at different times.

and airflow, and the viscous force of the airflow itself. It is the leading role of airflow return that the airflow field became totally stabilized in.

Particle trajectories. In this study, dust particles with diameters of $2\ \mu\text{m}$, $5\ \mu\text{m}$, and $30\ \mu\text{m}$ were taken as examples. Figure 3 shows the particle movement trajectories over time following the blasting processes.

As shown in Fig. 3, dust particles with different sized diameters were suspended in the air in the roadway from 0 to 10 m away from the working face. It was found that the blasting shock waves leading roles in the initial spraying velocities of the dust particles. In the areas located more than 10 m away from the working face, the wind-drag forces gradually played leading roles, rather than the blasting shock waves. The particles displayed obvious discrepancies in their movement trajectories due to the different gravity forces. The $2\ \mu\text{m}$ particles were too light to settle down naturally. Therefore, they moved upwards and continue floating due to the drag forces. The middle-sized dust particles ($5\ \mu\text{m}$) exhibited gradual sinking movement trajectories due to moderate gravity forces. Under the effects of the airflow, these particles moved forward along the upper position of the floor of roadway until being discharged^{25,26}. The coarse particles ($30\ \mu\text{m}$) settled rapidly to the floor due to the leading effects of sufficient gravity forces. The coarse particles then slid forward along the floor due to the wind-drag forces in the roadway. Eventually, due to friction forces, the coarse particle migration ceased to form dust retention.

$PM_{2.5}$ distributions. This research study observed the $PM_{2.5}$ distributions following the blasting processes at each time point, which were at 30, 60, 90, 120, 150, and 180 seconds, respectively. Figures 4 and 5 detail the $PM_{2.5}$ distributions at a breathing height of 1.5 m, and in the region of the 0.25 m upper and lower sections of the breathing height, respectively.

As shown in Fig. 4, within 30 seconds of the blasting, due to the strong blasting shock waves, large amounts of dust particle spray with high velocity were detected in the roadway space. During that time, high concentrations of dust particles in the $PM_{2.5}$ group passed across the blast working face. These dust particles posed serious threats to workers in the active working face. The dust particles in the front end of the dust group were not timely

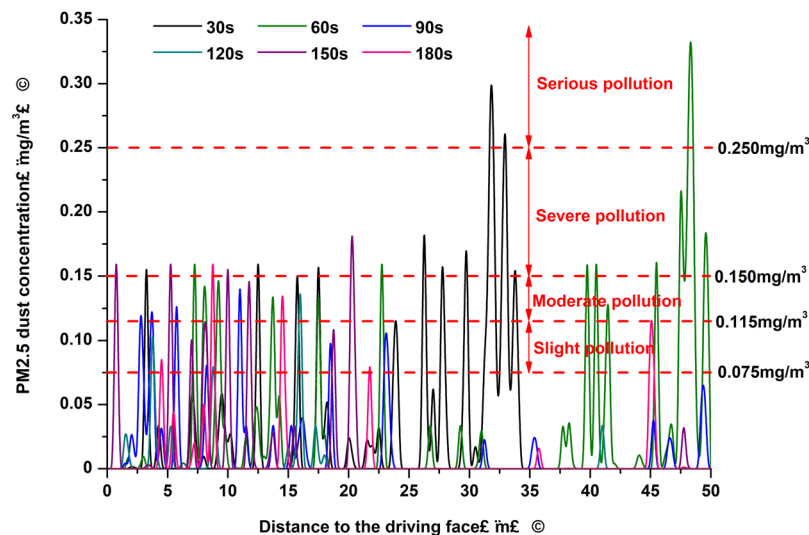


Figure 5. $PM_{2.5}$ concentrations along the roadway at the height of 1.5 m in the breathing zone.

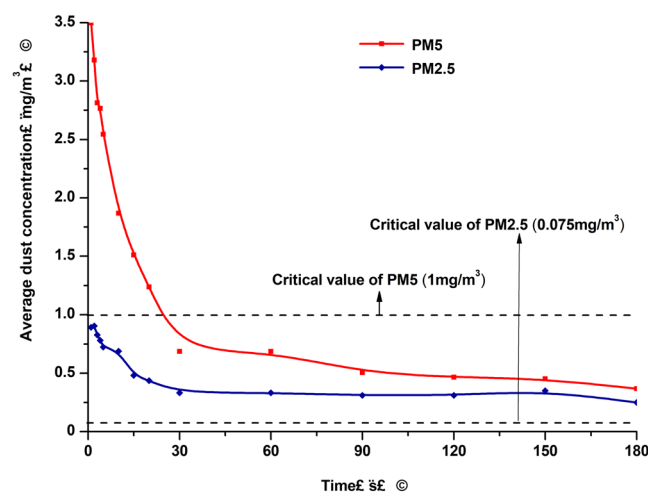


Figure 6. Comparison of the dust particle concentrations of the $PM_{2.5}$ and PM_5 .

and were effectively diluted. This concentration maintained a high level until being discharged. Meanwhile, the dust particles in the back end of the roadway were gradually diluted. These lower concentrations displayed stable distributions. This was mainly due to the higher airflow velocity in the front end of roadway, as shown in Fig. 2. As time passed, the dust particles in the high concentration areas were completely discharged from the roadway outlet as airflow. Eventually, only the $PM_{2.5}$ of lower concentration levels were suspended in the roadway space. Overall, the $PM_{2.5}$ represented alternately thin to dense distributions.

As shown in Fig. 5, the peak value of the $PM_{2.5}$ concentration was 0.33 mg/m^3 in the area 31.75 m away from the working face, at $t = 30$ seconds after blasting occurred. It was found to be 0.36 mg/m^3 at 48.25 m away from the working face, at $t = 60$ seconds. These findings presented serious pollution levels according to China's atmospheric quality standards. As time passed, the $PM_{2.5}$ accumulation zone with high concentrations gradually moved forward, and was fundamentally expelled from the roadway after approximately 60 seconds. At that point, the $PM_{2.5}$ concentrations started to slowly decline, and stabilized below 0.24 mg/m^3 . In the region located 0 to 25 m away from the working face, the $PM_{2.5}$ concentration remained at a high level. The fine dust was difficult to discharge as the airflow moved due to the vortex region located in that section, as shown in Fig. 2. At $t = 180$ seconds, the $PM_{2.5}$ concentrations located in parts of the roadway zones were still more than 0.075 mg/m^3 , and even more than 0.15 mg/m^3 , presenting moderate pollution levels.

Comparison of the dust concentration levels. Fig. 6 shows the statistical results of the average concentrations of $PM_{2.5}$ and PM_5 in the three-dimensional roadway following the blasting processes. As shown in Fig. 6, the PM_5 concentration after blasting was 3.5 mg/m^3 , which was approximately three to four times that of the $PM_{2.5}$. At 0 to 30 seconds after the blasting, the PM_5 and $PM_{2.5}$ concentrations had rapidly decreased. The decreased velocities of the PM_5 were obviously higher than that of the $PM_{2.5}$. After 30 seconds, the PM_5 concentration decreased relatively slowly, and maintained a downward trend. Meanwhile, the $PM_{2.5}$ concentrations had

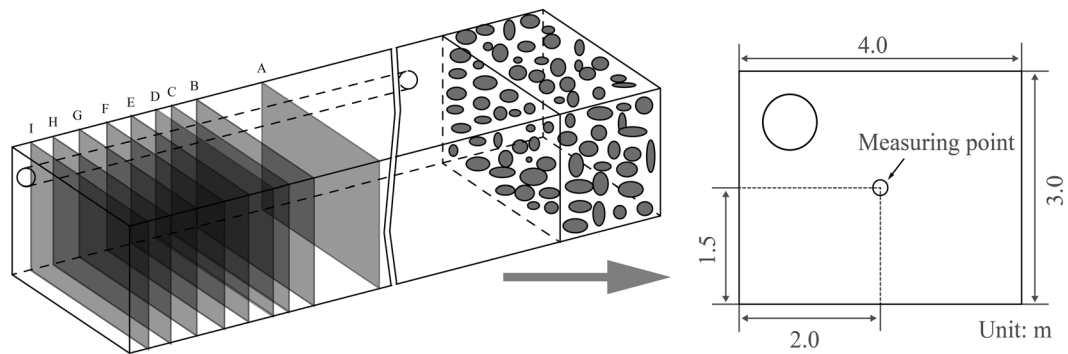


Figure 7. Diagram of the measurement point arrangement.

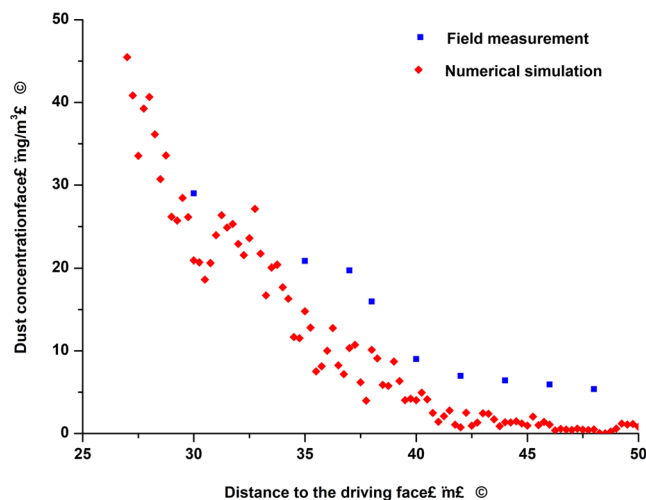


Figure 8. Comparison of the numeral and measured results.

only weakly declined or faintly undulated. As time continued to pass, the $PM_{2.5}$ and PM_5 concentrations both exhibited almost unchanged or extremely slow declining trends. Finally, the PM_5 concentrations stabilized at 0.5 mg/m^3 , which was below its critical value of 1 mg/m^3 . During the same period of time, the $PM_{2.5}$ concentrations stabilized at 0.3 mg/m^3 , which was well over its critical value of 0.075 mg/m^3 .

Verification of the numerical results. In order to verify the accuracy of this study's numerical results, the field data of a blast driven working face of the Wulan Coal Mine were measured. In accordance with the tunnel size and the arrangement of the production site, nine measuring points were set at nine cross-sections A, B, C, D, E, F, G, H, I with distances from the working face, at 30, 35, 37, 38, 40, 42, 44, 46, and 48 m, respectively, as shown in Fig. 7. All of the measuring points were fixed at heights of 1.5 m above the roadway floor, and at the same distances from the both sides of the roadway. It was difficult to precisely measure the lower $PM_{2.5}$ concentrations using a type of intrinsically safe extant dust detecting device. Also, the different sized dust particles exhibited similar dust concentration change tendencies^{26,27}. Therefore, the dust concentration data of all the dust in the working face of the Wulan Coal Mine were collected by the intrinsically safe extant dust detecting type device in this study. The data were measured within 180 seconds after the blasting processes occurred. A mine dust sampler (AKFC-92A, Zhengzhou Huazhi Electronic Technology Co., Ltd., China), was used in this study for the collection of the dust particles.

This study's comparison with the simulation results is illustrated in Fig. 8. As can be seen in the figure, the simulation results were found to be in good agreement with experimental data, which indicated an overall decreasing trend of the $PM_{2.5}$ concentrations along the roadway. Due to the influences of the personnel, devices, environment, and other factors, some deviations between the two results were found to exist. In fact, the $PM_{2.5}$ concentrations displayed a thick or dense alternation. This was determined to be mainly due to the smaller particle sizes and lighter masses of the $PM_{2.5}$ particles, as well as the easy movement under the action of the turbulent wind-drag forces. This study's mathematical model was determined to be accurate, and credible numerical results were obtained.

Conclusions

In this study, the following conclusions were obtained and summarized based on above results and discussion:

- (1) An obvious vortex region with a banded vortex center was found to exist in the front area of the underground roadway. The airflow velocity around the working face and close to the walls was significantly higher than that in the vortex center. The airflow field became gradually weakened along the roadway, and eventually stabilized.
- (2) The coarse dust particles rapidly realized natural sedimentation following the blasting processes. The medium-sized dust particles moved forward along the upper position of the floor, and were discharged before settling at the floor. The fine dust particles continue floating in the air of the roadway for a long period of time.
- (3) Following the blasting processes, the high-concentration PM_{2.5} areas located in the front end of the dust group were not quickly diluted. However, the PM_{2.5} particles at the back end of the underground roadway had been gradually diluted. These particles exhibited an overall alternating thin to dense phase distribution. When compared with the PM₅, the PM_{2.5} was found to be more difficult to discharge, which easily resulted in serious air pollution levels.

This study's simulation results offer a scientific basis for the formulation of a future concentration standard for PM_{2.5} dust particles in China's underground coal mine operations.

References

1. Xi, Z. *et al.* Experimental study on advantages of foam-sol in coal dust control. *Process Saf. Environ. Prot.* **92**(6), 637–644 (2013).
2. Rodgers, S. J. & Jayaraman, N. Control of respirable dust in conventional coal mining operations. *Proceedings of the Coal Mine Dust Conference, Morgantown, West Virginia*. 50–60 (1984).
3. Erol, I. *et al.* Pneumoconiosis and quartz content of respirable dusts in the coal mines in zonguldak, turkey. *Int. J. Coal Geol.* **116–117**, 26–35 (2013).
4. Weber, S. A. *et al.* Assessing the impact of fine particulate matter (pm_{2.5}) on respiratory-cardiovascular chronic diseases in the new york city metropolitan area using hierarchical bayesian model estimates. *Environ. Res.* **151**, 399–409 (2016).
5. Hsieh, Y. P., Bugna, G. & Robertson, K. Examination of two assumptions commonly used to determine pm_{2.5}, emission factors for wildland fires. *Atmos. Environ.* **147**, 274–283 (2016).
6. Woody, M. C. *et al.* Multiscale predictions of aviation-attributable pm_{2.5} for u.s. airports modeled using cmaq with plume-in-grid and an aircraft-specific 1-d emission model. *Atmos. Environ.* **147**, 384–394 (2016).
7. Hsu, C. H. & Cheng, F. Y. Classification of weather patterns to study the influence of meteorological characteristics on pm_{2.5} concentrations in yunlin county, taiwan. *Atmos. Environ.* **144**, 397–408 (2016).
8. Ballester, F., Tenías, J. M. & Pérezhoyos, S. Air pollution and emergency hospital admissions for cardiovascular diseases in valencia, spain. *Spain, J. Epidemiol. Community Health.* **55**(1), 57–65 (2001).
9. Nie, B. S. *et al.* Distribution of pm_{2.5} dust during mining operation in coal workface. *J. China Coal Soc.* **38**(1), 33–37(5) (2016).
10. Guo, H., Wang, F. & Wang, K. Preliminary study on pm_{2.5} standard for dust control in underground coal mine. *Saf. Coal Mines.* **46**, 174–177 (2015).
11. Gautam, S. *et al.* Characterization of pm_{2.5} generated from opencast coal mining operations: a case study of sonepur bazari opencast project of india. *Environ. Technol. Inno.* **6**, 1–10 (2016).
12. Tan, C. *et al.* Numerical simulation of influencing factors on dust movement during coal cutting at fully mechanized working faces. *Chinese J. Eng.* **36**(6), 716–721 (2014).
13. Nie, W. *et al.* The numerical simulation on the regularity of dust dispersion in whole-rock mechanized excavation face with different air-draft amount. *Procedia Eng.* **26**(4), 961–971 (2011).
14. Niu, W., Jiang, Z. & Tian, D. Numerical simulation of the factors influencing dust in drilling tunnels: its application. *Min. Sci. Technol. (China)*. **21**(1), 11–15 (2011).
15. Torano, J. *et al.* Auxiliary ventilation in mining roadways driven with roadheaders: validated cfd modelling of dust behaviour. *Tunn. Undergr. Space Technol.* **26**(1), 201–210 (2011).
16. Kurnia, J. C. *et al.* Dust dispersion and management in underground mining faces. *International Journal of Mining Science and Technology* **24**(1), 39–44 (2014).
17. Wang, X. Z. *et al.* Numerical simulation of distribution regularities of dust concentration during the ventilation process of coal roadway driving. *J. China Coal Soc.* **32**(4), 386–390 (2007).
18. Qin, Y. P. *et al.* Numerical simulation of dust migration and study on dust removal modes with the forced ventilation shunt in a fully mechanized workface. *J. Univ. Sci. Technol. B.* **33**(7), 790–794 (2011).
19. Nie, W. *et al.* Numerical simulation of swirl air curtain disturbed air-dust flowing field at hard rock fully mechanized workface. *Chin. Saf. Sci. J.* **24**(3), 120–125 (2014).
20. Chen, J. S., Wang, Y. & Jiang, Z. A. Numerical simulation of blasting dust concentration distribution and diffusion regularities in stope. *J. China Coal Soc.* **38**(6), 147–152 (2013).
21. Tsuji, Y., Tanaka, T. & Yonemura, S. Cluster patterns in circulating fluidized beds predicted by numerical simulation (discrete particle model versus two-fluid model). *Power Technol.* **95**(3), 254–264 (1998).
22. Levy, A. Two-fluid approach for plug flow simulations in horizontal pneumatic conveying. *Powder Technol.* **112**(3), 263–272 (2000).
23. Kawaguchi, T., Tanaka, T. & Tsuji, Y. Discrete particle simulation of plug conveying in a vertical pipe, In: *Proceedings of 6th international conference on Bulk Materials Storage, Handling and Transportation. Australia: The Institution of Engineering.* 321–327(1998).
24. Hoomans, B. P. B. Granular dynamics of gas-solid two-phase flows. Universiteit Twente. (2000)
25. Liu, Q. *et al.* The effects of the installation position of a multi-radial swirling air-curtain generator on dust diffusion and pollution rules in a fully-mechanized excavation face: A case study. *Powder Technol.* **329**(15), 371–385 (2018).
26. Wang, H. *et al.* Effects of air volume ratio parameters on air curtain dust suppression in a rock tunnel's fully-mechanized working face. *Advanced Power Technol.* **29**(2), 230–244 (2018).
27. Yu, H. *et al.* Mechanisms of dust diffuse pollution under forced-exhaust ventilation in fully-mechanized excavation faces by CFD-DEM. *Powder Technol.* **317**(15), 31–47 (2017).

Acknowledgements

This research was supported by the National Natural Science Foundation of China (51504160, 51574172), the Joint Funds of the National Natural Science Foundation of China (U1710258, U1710121). This work is also a project supported by the Training Program of First-class Discipline for Young Academic Backbone of Taiyuan University of Technology.

Author Contributions

G.F. and S.H. conceived and designed the research. Q.L. and S.H. performed the research. Q.L. and S.H. analyzed the data. G.F. wrote the main manuscript text. All authors discussed the results and critically reviewed the manuscript.

Additional Information

Competing Interests: The authors declare no competing interests.

Publisher's note: Springer Nature remains neutral with regard to jurisdictional claims in published maps and institutional affiliations.



Open Access This article is licensed under a Creative Commons Attribution 4.0 International License, which permits use, sharing, adaptation, distribution and reproduction in any medium or format, as long as you give appropriate credit to the original author(s) and the source, provide a link to the Creative Commons license, and indicate if changes were made. The images or other third party material in this article are included in the article's Creative Commons license, unless indicated otherwise in a credit line to the material. If material is not included in the article's Creative Commons license and your intended use is not permitted by statutory regulation or exceeds the permitted use, you will need to obtain permission directly from the copyright holder. To view a copy of this license, visit <http://creativecommons.org/licenses/by/4.0/>.

© The Author(s) 2018